Nanobiosensors: Designing Approach and Diagnosis

38

Masoud Negahdary and Lúcio Angnes

Contents

Abstract

In this chapter, we evaluated electrochemical biosensors designed to diagnose various diseases. The biorecognition elements in these biosensors consisted of antibodies, aptamers, and peptides. The studied biosensors used different nanomaterials (nanoparticles, nanostructures, nanocomposites, and other nano-based materials) to amplify the output signals and increase the diagnostic sensitivity. Here, all efforts were made to review and introduce the latest related research. The classification of the included biosensors was based on the type of biorecognition element and the type of analyte related to each type of disease, where a number of them were evaluated and reviewed in detail. Other designed biosensors related to each defined section have also been presented in several tables. Complete details of each biosensor have been offered in the tables. The final sections of this chapter provide a brief overview of the importance, prospects, and future of these biosensors.

M. Negahdary · L. Angnes (✉)
Department of Fundamental Chemistry, Institute of Chemistry, University of São Paulo, São Paulo, Brazil
e-mail: luangnes@iq.usp.br

U. P. Azad, P. Chandra (eds.), *Handbook of Nanobioelectrochemistry*,
https://doi.org/10.1007/978-981-19-9437-1_38

Keywords

Nanomaterial-based biosensors · Immunosensors · Aptasensors · Peptide-based biosensors · Macromolecules · Electrochemical detection · Bioanalysis

1 Introduction

The use of new technologies is an important achievement in the rapid and accurate diagnosis of various diseases (Choudhary et al. 2016; Mahapatra et al. 2020). *Biosensors* are devices that respond to the presence of a particular substance (analyte) in an environment and produce measurable signals (Felix and Angnes 2018; Negahdary 2020a, b; Negahdary et al. 2020). A biosensor is composed of (at least) three parts: a biorecognition element, a signal transducer, and a detector. The analyte recognized by a biosensor comprises a wide range of chemical or biological substances, such as small organic molecules, peptides, proteins, nucleic acids, carbohydrates, tissue, or whole cells (Bakshi et al. 2021; Rong et al. 2021; Zhao et al. 2021; Yang et al. 2021; Zhang et al. 2021b; Abrego-Martinez et al. 2022; Bhatnagar et al. 2018; Shanbhag et al. 2021). The most selective biorecognition elements more recently introduced for biosensors include antibodies, aptamers, and peptide sequences. Ideally, this component should have a high affinity (low limit of detection (LOD)), high selectivity (minimum interference effect), wide dynamic range, and short response time (Negahdary and Heli 2019a; Heiat and Negahdary 2019; Negahdary et al. 2019a; Negahdary and Heli 2019b; Taheri et al. 2018; Chandra et al. 2012). A signal transducer can convert a molecular recognition event into a measurable signal such as fluorescence, chemiluminescence, colorimetric, or electrochemical/electrical outputs (Öndeş et al. 2021b; Song et al. 2021; Amouzadeh Tabrizi et al. 2021). The selection of signal transducer depends on other considered biosensor components and the type of detection technique(s).

In this chapter, our emphasis is on diagnosing diseases using electrochemical techniques. Biosensors equipped with various nanomaterials have recently provided efficient diagnoses for many acute and chronic diseases (Negahdary and Heli 2018; Negahdary 2020a, b; Mahato et al. 2018). The combination of biorecognition elements with nanomaterials, or the modification of the surface of the signal transducers with nanomaterials, has created biosensors with higher sensitivity and specificity (Pumera et al. 2007; Mahato et al. 2019). The purpose of designing and using nanobiosensors to diagnose various diseases is to reach a faster diagnosis, higher sensitivity, more accessible (portable), and less expensive application.

The available detection methods to diagnose various diseases often have several challenges to be overcome, such as lowering their cost, decreasing the time for each analysis, simplifying complicated diagnostic procedures, improving their specificity, and minimizing the effect of interfering agents (Gooding 2006; Morales and Halpern 2018).

One of the long-term goals of nanobiosensors design is to provide sensitive, selective, and portable diagnostic tools that will offer early diagnosis and

subsequently accelerate therapeutic procedures. Nanobiosensors have great potential for important applications to diagnose many diseases, among them myocardial infarction (MI), cancers, and so on, that can save the lives of thousands of patients each year and significantly reduce the treatment costs (Negahdary and Heli 2019a, b; Heiat and Negahdary 2019; Negahdary et al. 2019a; Taheri et al. 2018). Because it is clear that rapid diagnosis of diseases increases the likelihood of treatment and rescue of patients, the rapid diagnosis of diseases in the early stages can also reduce treatment costs. Nanobiosensors can also be used to diagnose and monitor the status of diseases such as cancers (Heiat and Negahdary 2019).

In this chapter, we investigated the application of electrochemical nanobiosensors in the diagnosis of various diseases. It should be noted that three essential biorecognition elements used to build nanobiosensors (antibodies, aptamers, and peptides) and also analytes have been applied for the classification. This chapter covers the recent primary efforts to design electrochemical nanobiosensors (immunosensors, aptasensors, and peptide-based biosensors) to diagnose various diseases, all the articles being discussed here, whereas the most of included researches was published in 2020–2021. It is hoped that our presentation in this chapter can be used as guiding content for the design of new electrochemical nanobiosensors.

2 Applications of the Electrochemical Nano Immunosensors in the Early Diagnosis of Diseases

The most decisive laboratory test for diagnosing MI and myocardial injury is the accurate measurement of troponin (Chapman et al. 2020). Troponin contains a set of three protein subunits (Troponin T (TnT), Troponin I (TnI), and Troponin C (TnC)). Assays of TnI and TnT are considered the gold standard of MI diagnosis when patients with clinical signs are referred to the emergency units (Reichlin et al. 2009). Figure 38.1 shows the three-dimensional structure of the troponin complex (Shave et al. 2010). The subunits of this protein form a complex that regulates the interaction between actin and myosin, which plays an essential role in the contractions of various muscles, including the heart muscle. In the muscle contraction/relaxation process, the three subunits – the calcium-binding component (TnC), the inhibitory component (TnI), and the tropomyosin-binding component (TnT) – perform complementary roles (Katrukha 2013).

The European society of cardiology (ESC) and the American college of cardiology (ACC) have also considered minor myocardial ischemia as MI. In fact, due to the high diagnostic specificity of the troponin biomarker in the first days after a MI, as well as the direct relationship between the amount of troponin released from myocardial muscle and necrotic area into the circulation and the high stability of this biomarker in the blood (8–14 days), this biomarker is considered as the best preferred-biomarker for diagnosis of MI (Mair et al. 2018; Chapman et al. 2020; Negahdary et al. 2017, 2018, 2019a, b; Negahdary 2020a; Negahdary and Heli 2019a).

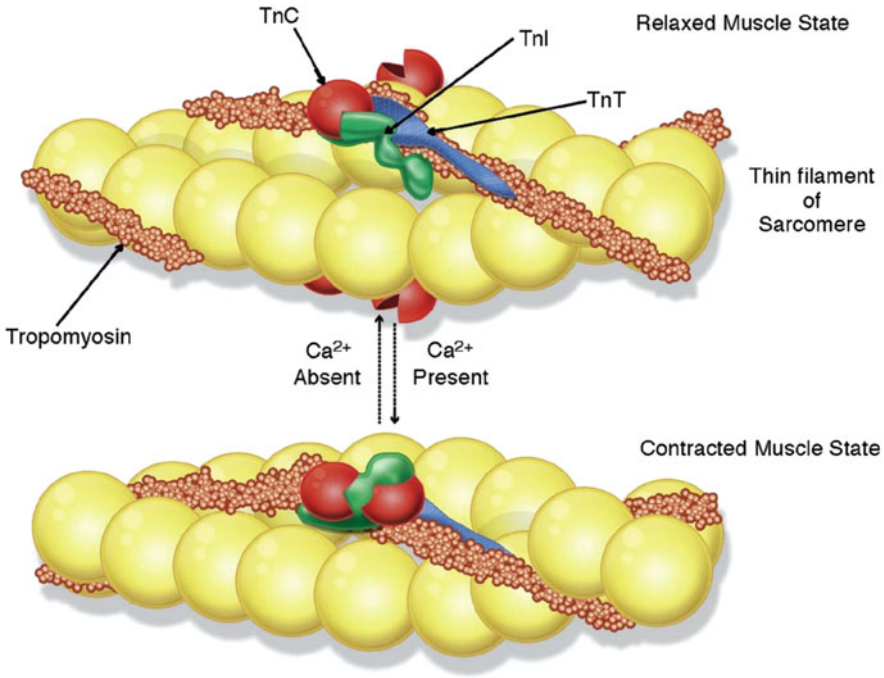

Fig. 38.1 Three-dimensional structure of the troponin complex in the process of muscle relaxation and contraction. (Reproduced with permission from Shave et al. (2010))

In a research, an immunosensor was designed for detection of TnI using a modified glassy carbon electrode (GCE) with AuPtPd porous fluffy-like nanodendrites (AuPtPd FNDs) (Cen et al. 2021). Here, as one of the initial procedures, AuPtPd FNDs were synthesized. First, 50 mmol L^{-1} thymine was dissolved in water, and then by using 1 M NaOH, the pH of this solution was increased to 10. Afterward, the temperature of the mentioned solution was elevated to 60 °C, and then 24.3 mmol L^{-1} $HAuCl_4$, 38.6 mmol L^{-1} H_2PtCl_6, and 100 mmol L^{-1} H_2PdCl_4 were added. This mixture was kept at the mentioned temperature for 20 min (Fig. 38.2). At the next step, 100 mmol L^{-1} L-ascorbic acid (AA) was added and stirred, and the achieved mixture was kept at room temperature for 12 h. Finally, the product was centrifuged and dried at 60 °C. In order to design an immunosensing platform, a defined amount of AuPtPd FNDs was dissolved in the deionized water, and a drop of this suspension was transferred to the GCE surface (the signal transducer). The suspension on the surface of GCE was dried at room temperature naturally. At the next step, a defined concentration of TnI antibody as the biorecognition element was immobilized on the surface of GCE-AuPtPd FNDs, and the unwanted binding sites of antibody molecules were blocked by bovine serum albumin (BSA) (Fig. 38.2). Finally, the prepared biosensor was immersed in the various concentrations of TnI as the analyte. The electrochemical assays were

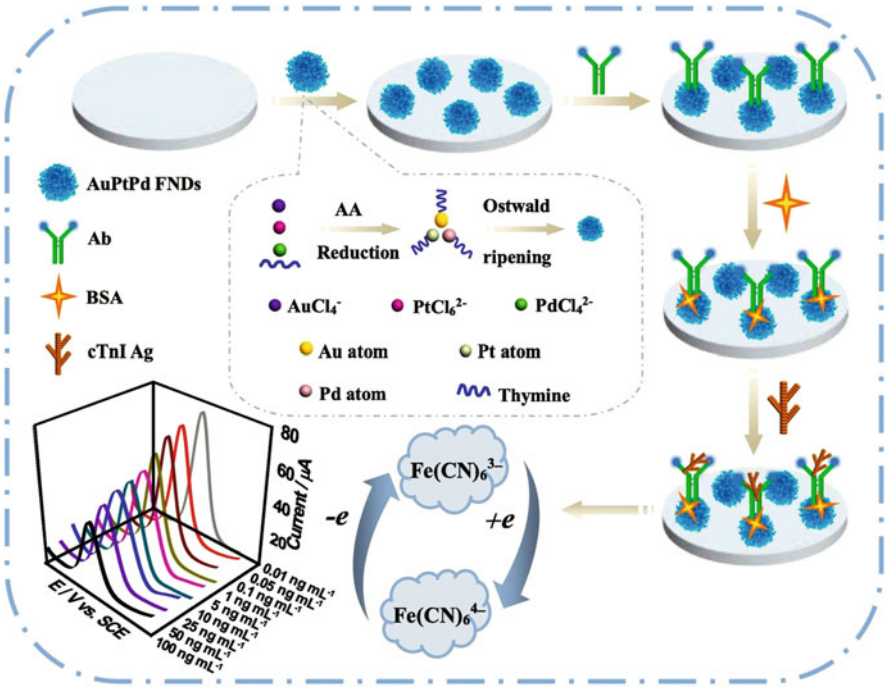

Fig. 38.2 An immunosensor designed to diagnose TnI using a modified GCE with AuPtPd FNDs. (Reproduced with permission from Cen et al. (2021))

followed using differential pulse voltammetry (DPV) in the presence of $[Fe(CN)_6]^{3-}$ as the redox marker while the counter and references electrodes were platinum and saturated calomel, respectively. The presence of TnI led to the decrease of DPVs peak current. At this condition, the signal decrease was related to the electrode surface's reduced free area and the increment of analyte concentrations. This signal-off immunosensor could detect TnI in a linear range from 0.01 to 100.0 ng mL^{-1}, and the reported LOD was about 3 pg mL^{-1}.

Carcinoembryonic Antigen (CEA) is a glycoprotein tumor marker produced in the fetal gastrointestinal tract. Its levels before birth reach maximum but decline immediately after birth. In the early 1960s, it was discovered that CEA was present in the blood of adults with colorectal tumors and was initially thought the CEA to be specific for colorectal cancer (Tang et al. 2020; Pishvaian et al. 2016; Xiang et al. 2013). It was then discovered that this tumor marker is present in patients with a variety of carcinomas (cancers related to liver, bile duct, breast, and pancreas), sarcomas, and even many benign diseases (colitis, diverticulitis, and cholecystitis) and especially liver diseases such as cirrhosis and hepatitis is also present with high levels (Al-Kazzaz and Dr 2015; Al-Mudhaffar and Dr 2017). This tumor marker is used to determine the severity and prognosis of several types of cancers, as well as to control and monitor several diseases. Smokers also have high levels of CEA. In

general, its levels should generally be less than 5 ng mL^{-1} (Sajid et al. 2007; Tang et al. 2007); otherwise, its level is abnormal. This tumor marker has the highest possible level in metastasis and also in failed treatment of liver and bone cancers. By measuring the level of this antigen, the patients can be informed about several possible cancers in various stages.

In a study, an immunosensor was developed for early detection of CEA using a modified GCE with $ZnMn_2O_4$@rGO nanocomposite and Au NPs (Fan et al. 2021). As the first step, $ZnMn_2O_4$@rGO nanocomposite was synthesized by the following procedure: The GO solution was mixed with ethylene glycol and then ultrasonicated. Afterward, the obtained suspension was mixed with the defined concentrations of urea, $MnCl_2{\cdot}4H_2O$, and $ZnCl_2$ and then inserted in an oil bath and kept at 200 °C for 24 h. Then, the filtration was performed, and the mixture was kept at 60 °C for 12 h. Finally, the material was calcined at 600 °C for 2 h under N_2 atmosphere, and the $ZnMn_2O_4$@rGO nanocomposite was achieved. In order to set up the CEA immunosensing platform, a GCE was applied as the signal transducer and modified with the prepared 15 mg mL^{-1} $ZnMn_2O_4$@rGO nanocomposite by immersing the working electrode in the related nanostructure solution. At the next step, the GCE-$ZnMn_2O_4$@rGO nanocomposite was modified with Au NPs through an electrodeposition procedure (V: −0.2 V, time: 30 s). The Au NPs synthesis solution consisted of 5 mmol L^{-1} $HAuCl_4$ and 0.01 M Na_2SO_4. Subsequently, a CEA-specific antibody as the biorecognition element was immobilized on the surface of the modified GCE with $ZnMn_2O_4$@rGO nanocomposite and Au NPs. Then, the unwanted binding sites of the antibody on the surface of GCE were blocked by using the BSA solution. Finally, the prepared immunosensor was evaluated in the presence of various concentrations of the analyte. All the electrochemical measurements were followed using a three-electrode system; the mentioned GCE was the working, and platinum and Ag/AgCl electrodes were applied as the counter and reference, respectively. The electrochemical assays were followed by the DPV as the detection technique and supported by $[Fe(CN)_6]^{3-/4-}$ as the redox marker. This electrochemical immunosensor could detect CEA in a linear range from 0.01 to 50 ng mL^{-1}, and the reported LOD was equal to 1.93 pg mL^{-1}.

Prostate-specific antigen (PSA) is a protein produced primarily by prostate cells (Wu et al. 2001). The prostate is a small gland that produces part of the seminal fluid. Most of the PSA produced is excreted through the seminal fluid, and some other amounts enter the bloodstream. PSA is present in the blood in two forms, free and complex (bound with a protein) (Nordström et al. 2018). Usually, all men have a small amount of PSA in their blood. Elevated PSA levels may be a sign of a prostate problem. In more than 80% of men with prostate cancer, PSA levels are higher than 4 ng mL^{-1} (Raouafi et al. 2019). However, levels above 4 ng mL^{-1} are not always associated with cancer. The PSA assay may be used as a promising tumor marker to screen and monitor prostate cancer. The goal of screening is to diagnose prostate cancer until the cancer cells are still in the prostate and have not spread (metastasis) to other organs (Romesser et al. 2018; Spratt et al. 2018). High increases in PSA levels in the blood are usually associated with prostate cancer but may also be associated with prostatitis and benign prostatic hyperplasia (BPH) (Fadila et al.

2020; Logozzi et al. 2019). It was also observed that, with age, PSA levels in all men usually increase.

With age, the weight of the prostate increases, and this enhanced size mostly leads to BPH or prostate cancer. As an outcome, the risk of prostate cancer increases with age (Boeri et al. 2021; Butler et al. 2020). If prostate cancer is diagnosed in the early stages (when still limited), generally it is not fatal, and with surgery or radiotherapy, the patients will have about 95% survival rate. However, in the late stages, when metastasis has occurred and other organs such as lymph nodes, bones, liver, and lungs are also affected, the life span after hormone therapy is only about 2 years (Hassanipour et al. 2020; de Crevoisier et al. 2018; Smith et al. 2018). Therefore, the initial diagnosis of prostate cancer is essential. Today, electrochemical biosensors have been used as valuable tools in the early detection of PSA (Sattarahmady et al. 2017; Negahdary et al. 2020; Rahi et al. 2016; Yazdani et al. 2019; Felix and Angnes 2018).

A very effective immunosensor was built on a fluorine-doped tin oxide (FTO) electrode modified with Au nanorods (NRs)-reduced-graphene oxide (rGO) nanocomposite as the signal transducer and was used to determine many concentrations of PSA (Chen et al. 2021c). First, Au NRs were synthesized. A solution of 1 mmol L^{-1} $HAuCl_4$ was prepared and then reduced by 0.01 mol L^{-1} $NaBH_4$. In this way, the seed solution of Au was obtained. Then, 0.1 mol L^{-1} cetyltrimethylammonium bromide (CTAB) and 1 mmol L^{-1} $HAuCl_4$ were mixed and then heated at 60 °C for 30 min; afterward, 2 M HCl and 10 mmol L^{-1} $AgNO_3$ were added to the prepared mixture and stirred for 2 min. Finally, the prepared seed solution of Au was added to the mixture, and after 300 min, Au NRs were achieved. In another procedure, GO was produced based on the Hummers method by applying graphite powder. Then, a defined concentration (2 mg mL^{-1}) of the produced rGO mixed with 0.2 mg mL^{-1} Au NRs and led to producing Au NRs-rGO nanocomposite. In order to develop the immunosensing platform, an FTO electrode was considered as the working electrode and modified with Au NRs-rGO nanocomposite (Fig. 38.3). Afterward, FTO-Au NRs-rGO was modified with chitosan to enhance the

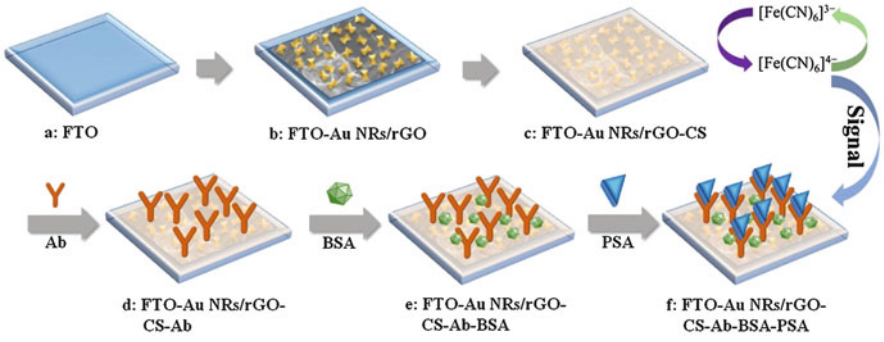

Fig. 38.3 An immunosensor for detection of PSA by applying a modified FTO electrode with Au NRs-rGO nanocomposite. (Reproduced with permission from Chen et al. (2021c))

biocompatibility and stability of the used nanocomposite on the surface of the FTO electrode. At the next step, a considered PSA antibody as the biorecognition element was dropped on the surface of the working electrode, and then the unspecified binding sites of the immobilized antibody were blocked by BSA. Finally, the prepared immunosensor was applied to detect the various concentrations of PSA (Fig. 38.3). The electrochemical assays were followed using the DPV technique and via a three-electrode system where the modified FTO, platinum, and saturated calomel electrodes were applied as the working, counter, and reference, respectively. The principle of detection was based on the changes found between the electron transfer rates. In the absence of PSA, the electron transfer rate was at the maximum value, but in the presence of the analyte, the bound status between the antibody and analyte led to blocking the electron transfer rate along with the increment of PSA concentrations. So, the lowest DPV peak current was found at the highest concentration of the analyte. This signal-off immunosensor detected PSA in a range from 0.1 to 150 ng mL^{-1}, and the reported LOD was equal to 0.016 ng mL^{-1}.

In Table 38.1, comprehensive details for nanoimmunosensors designed to diagnose various diseases have been provided.

3 Applications of the Electrochemical Nano and Peptide-Based Biosensors in the Early Diagnosis of Diseases

A peptide-based biosensor was developed for early detection of TnI by applying a mercury film-modified screen-printed electrode as the transducer (Xie et al. 2021). For this electrochemical biosensor, the peptide-oligonucleotide conjugate (POC)-templated quantum dots (QDs) (POC@QDs) were first synthesized. In order to synthesize this nanocomposite, the sodium hydrogen telluride (NaHTe) solution was prepared. Afterward, another solution containing 100 μmol L^{-1} POC, 1.25 mmol L^{-1} $CdCl_2$, and 1.05 mmol L^{-1} glutathione was prepared and mixed with the NaHTe solution. The pH of the obtained mixture was adjusted to 9, and then the temperature was increased to 100 °C for 5 min and then cooled slowly. Finally, the precipitation occurred after centrifuging, and the phosphate buffer solution (PBS) was applied to provide a resuspended POC@QDs nanocomposite when needed. In order to setup this biosensor, 4 mg mL^{-1} magnetic beads were functionalized with streptavidin and were mixed with a PBS solution containing 2 μmol L^{-1} of a peptide sequence (FYSHSFHENWPS) as the biorecognition element and incubated at room temperature for 120 min. Then, the purification of peptide-functionalized magnetic beads (Pep@MBs) nanocomposite was followed and then resuspended in the PBS solution. At the next step, a mixture containing a defined concentration of TnI (analyte), POC@QDs, and Pep@MBs was prepared and incubated at 37 °C for 45 min to produce the biosensing structure as a sandwich form (QDs@cTnI@MBs). Before the electrochemical measurements, MBs molecules were removed, and the remaining solution was mixed with 0.5 M nitric acid to release Cd^{2+} and subsequently mixed with 0.2 M HAc-NaAc buffer (pH 5.2). In order to present the biosensing principle of this electrochemical peptide-based biosensor, it should be

Table 38.1 The features and details about applied components in recent developed electrochemical nanoimmunosensors for diagnosis of diseases

Analyte	Transducer	Nanomaterial (s)	Redox marker	Detection technique (s)	Detection range	LOD	Ref.
Epithelial growth factor receptor (EGFR)	GE	Gold nanostructure	$[Fe(CN)_6]^{3-/4-}$	DPV	10 pg mL^{-1}–100 ng mL^{-1}	6.9 pg mL^{-1}	Bakshi et al. (2021)
PSA	FTO electrode	Au NRs-rGO composite	$[Fe(CN)_6]^{3-/4-}$	DPV	0.1–150 ng mL^{-1}	0.016 ng mL^{-1}	Chen et al. (2021c)
Alpha-fetoprotein (AFP)	Screen-printed electrode (SPE)	Ordered mesoporous carbon (OMC)@Au NPs	$[Fe(CN)_6]^{3-/4-}$	DPV	10 fg mL^{-1}–100 ng mL^{-1}	3.33 fg mL^{-1}	Rong et al. (2021)
Carbohydrate antigen 19-9 (CA19-9)	GCE	Multiwalled carbon nanotube and magnetite nanoparticle (MWCNT-Fe_3O_4)	$[Fe(CN)_6]^{3-/4-}$	SWV	1.0 pg mL^{-1}–100 ng mL^{-1}	0.163 pg mL^{-1}	Kalyani et al. (2021)
Interleukin-6	ITO	Acetylene black (AB)	$[Fe(CN)_6]^{3-/4-}$	EIS	0.01–50 pg mL^{-1}	3.2 fg mL^{-1}	Aydin et al. (2021b)
SARS-CoV-2	SPE	Magnetic beads (MBs)	N,N-dimethylformamide	DPV	S protein: 0.04–10 μg mL^{-1} N protein: 0.01–0.6 μg mL^{-1}	S protein: 19 ng mL^{-1} N protein: 8 ng mL^{-1}	Fabiani et al. (2021)
TnI/C-reactive protein (CRP)/ procalcitonin (PCT)	Transparency film screen-printed-based electrode	GO	$[Fe(CN)_6]^{3-/4-}$	SWV	TnI: 0.001–250 ng mL^{-1} CRP: 1–1000 ng mL^{-1} PCT: 0.0005–250 ng mL^{-1}	TnI: 0.16 pg mL^{-1} CRP: 0.38 ng mL^{-1} PCT: 0.27 pg mL^{-1}	Boonkaew et al. (2021)

(continued)

Table 38.1 (continued)

Analyte	Transducer	Nanomaterial (s)	Redox marker	Detection technique (s)	Detection range	LOD	Ref.
Human parathyroid hormone (PTH)	Screen-printed carbon electrode (SPCE)	Multiwalled carbon nanotube (MWCNT)/Au NPs	$[Fe(CN)_6]^{4-}$	DPV/SWV	DPV: 10^3–3×10^5 fg mL^{-1} SWV: 10^3–3×10^5 fg mL^{-1}	DPV: 0.886 pg mL^{-1} SWV: 0.065 pg mL^{-1}	Chen et al. (2021a)
Hunger hormone ghrelin (GHRL)	SPE	HfO_2-Pr_6O_{11} nanomaterials	$[Fe(CN)_6]^{3-/4-}$	DPV	0.01 pg mL^{-1}–50 ng mL^{-1}	0.006 pg mL^{-1}	Sun et al. (2021)
CCR4 antigen	ITO	Acid-substituted poly (pyrrole) polymer	$[Fe(CN)_6]^{3-/4-}$	EIS	0.02–8 pg mL^{-1}	6.4 fg mL^{-1}	Aydin et al. (2021a)
Procalcitonin (PCT)	GCE	PtCoIr nanowires/ SiO_2@Ag NPs	$[Fe(CN)_6]^{3-/4-}$	DPV	0.001–100 ng mL^{-1}	0.46 pg mL^{-1}	Wang et al. (2021d)
PSA	SPE	Sulfur-doped graphene QDs@gold nanostar (S-GQDs@Au NS)	$[Fe(CN)_6]^{3-/4-}$	LSV	10 fg mL^{-1}–50 ng mL^{-1}	0.29 fg mL^{-1}	Tran et al. (2021)
Cancer antigen 125 (CA125)	SPE	Boron nitride (BN) nanosheets	$[Fe(CN)_6]^{3-/4-}$	DPV	5–100 U	1.18 U mL^{-1}	Öndeş et al. (2021a)
IgG	SPCE	Graphene-TiO_2	$[Fe(CN)_6]^{3-}$	EIS	62.5–2000 ng mL^{-1}	2.81 ng mL^{-1}	Siew et al. (2021)
Hepatitis B surface antigen (HBsAg)	ITO	Fe_3O_4 NFs	$[Fe(CN)_6]^{3-/4-}$	DPV	0.5 pg mL^{-1}–0.25 ng mL^{-1}	0.16 pg mL^{-1}	Wang et al. (2021b)

TnI	GCE	AuPtPd porous fluffy-like nanodendrites (AuPtPd FNDs)	$[Fe(CN)_6]^{3-}$	DPV	0.01–100 ng mL^{-1}	3 pg mL^{-1}	Cen et al. (2021)
CEA	GCE	Silica coated nickel/carbon ($Ni/C@SiO_2$) nanocomposites/gold nanoparticle-coated PANI microsphere (CPS@PANI@Au NPs)	$[Fe(CN)_6]^{3-/4-}$	DPV	0.006–12 ng mL^{-1}	1.56 pg mL^{-1}	Tian et al. (2021a)
PSA	GCE	Poly(indole-6-carboxylic acid) (PICA) nanowire	6-PICA	SWV	0.5–100 ng mL^{-1}	0.11 ng mL^{-1}	Martínez-Rojas et al. (2021)
Carbohydrate antigen 15-3 (CA15-3)	GCE	PtCo alloyed nanodendrites (PtCo NDs)	$[Fe(CN)_6]^{3-/4-}$	DPV	0.1–200 U mL^{-1}	0.0114 U mL^{-1}	Ge et al. (2021)
PSA	GCE	MWCNT-Fe_3O_4 nanocomposite	$[Fe(CN)_6]^{3-/4-}$	DPV	2.5 pg mL^{-1}–100 ng mL^{-1}	0.39 pg mL^{-1}	Shamsazar et al. (2021)
CEA	GCE	$ZnMn_2O_4$@rGO/Au NPs	$[Fe(CN)_6]^{3-/4-}$	DPV	0.01–50 ng mL^{-1}	1.93 pg mL^{-1}	Fan et al. (2021)

noted that POC and analyte contained trypsin substrate in their sequences and in the sandwich structure of QDs@cTnI@MBs when trypsin was applied, QDs molecules were released through a proteolysis process. The release of QDs led to producing more Cd^{2+} molecules and enhancement of the output electrochemical DPVs. The releasing amount of QDs from the sandwich structure had a direct relationship with the concentration of TnI. This signal-on peptide-based biosensor detected TnI in a linear range from 0.001 to 100 ng mL^{-1} while the reported LOD was about 0.42 pg mL^{-1}.

In another research, a PSA biosensor was developed based on an antibody-peptide sandwich platform by applying a modified GCE with Au@PDA@BCN nanocomposite as the signal transducer (Zheng et al. 2021). Initially, boron-doped carbon nitride (BCN) nanosheets were synthesized by the one-step calcination procedure. Here, 5 g 4-pyridylboronic acid was transferred to a corundum boat and heated at 800 °C for 180 min. Afterward, a core-shell substrate (polydopamine (PDA)@BCN) was produced by mixing BCN and dopamine in a 100 mmol L^{-1} Tris-HCl buffer. This mixture was then sonicated (30 min), stirred, and centrifuged to produce PDA@BCN nanocomposite. At the next step, to produce Au@PDA@BCN nanocomposite, Au NPs were synthesized from $HAuCl_4$ by applying the sodium citrate reduction procedure. Then, a defined concentration of PDA@BCN and Au NPs were mixed and stirred at 4 °C for 4 h and subsequently centrifuged and washed with deionized water. Finally, the required amount of the synthesized Au@PDA@BCN nanocomposite was dispersed in the deionized water and kept in the refrigerator for future use.

In other synthesizing procedures, covalent organic framework (COF), MnO_2@COF, and AuPt@MnO_2@COF were synthesized. The solvothermal method was applied for synthesizing the COF by mixing 1,2,4,5-Tetrakis-(4-formylphenyl) benzene (TFPB) and 1,4-diaminobenzene (PPDA). This mixture was ultrasonicated, and then 6 M acetic acid was added and filled in an oil bath to follow the required reactions at 120 °C for 3 days. The product was washed with tetrahydrofuran and acetone, and the COF was achieved. At the next step, to synthesize MnO_2@COF, required amounts of solid COF and $HClO_4$ were added in the deionized water and sonicated for 10 min. Afterward, the temperature of the mixture was adjusted at 30 °C, and then a defined amount of $KMnO_4$ was added. This mixture was then stirred, sonicated, and centrifuged, respectively. The final product was washed with deionized water, and the MnO_2@COF as a powder was obtained using freeze-drying.

AuPt@MnO_2@COF nanocomposite was produced by the $NaBH_4$ reduction method. In this synthesizing method, MnO_2@COF was mixed with ethanol and then sonicated. At the next step, $HAuCl_4$ and H_2PtCl_6 were added to the above mixture and sonicated for 60 min. Finally, the $NaBH_4$ was added to the mixture and then was sonicated and centrifuged. The AuPt@MnO_2@COF was attained and, based on the required concentration, was resuspended in PBS solution. Subsequently, a bioconjugated structure (peptide/methylene blue/AuPt@MnO_2@COF) was produced. First, 2.5 mg mL^{-1} MB and 2 mg mL^{-1} AuPt@MnO_2@COF nanocomposite solutions were prepared, then mixed, and kept under stirring for

12 h. Afterward, the mixture was centrifuged and then washed with deionized water to remove extra methylene blue. At this moment, methylene blue/AuPt@MnO_2@COF nanocomposite was obtained and dispersed into the PBS solution. Finally, 1 mg mL^{-1} PSA peptide (CGGGGMERCPIKMFYNLGSPYMNI) was added to the final mixture and stirred at 4 °C for 12 h. The centrifuge and washing with PBS solution provide the peptide/methylene blue/AuPt@MnO_2@COF bioconjugated structure.

In order to set up the biosensing platform, a GCE was applied as the working electrode and then modified with Au@PDA@BCN nanocomposite. Afterward, the PSA antibody as one part of the biorecognition element was added on the surface of the GCE-Au@PDA@BCN nanocomposite, and then the unwanted and unspecified antibody binding sites were blocked by BSA. Subsequently, the considered concentrations of analyte were prepared and dropped on the surface of the signal transducer. Finally, the prepared bioconjugated structure (peptide/methylene blue/AuPt@MnO_2@COF) was added. So, the analyte was located in a sandwich structure between the antibody and peptide (antibody-analyte-peptide). The electrochemical assays were followed by the DPV technique while the applied methylene blue molecules in the bioconjugated structure contributed as the redox marker. The electrochemical behavior of this biosensor confirmed that after modification of the surface of GCE with Au@PDA@BCN nanocomposite due to the increased active surface area, the DPV peak current was increased. After immobilization of the PSA antibody and PSA, the DPVs peak currents were reduced regularly based on the blocking of the electron transfer rate. However, after immobilization of the bioconjugated structure on the surface of the signal transducer, the DPV peak current increased again due to the high conductivity of AuPt NPs. This antibody-peptide sandwich-based PSA signal-on biosensor could detect this cancer biomarker in a linear range from 0.00005 to 10 ng mL^{-1}, and the found LOD was about 16.7 fg mL^{-1}.

In another research, a CEA biosensor was developed by applying a modified ITO electrode with polyaniline (PANI) and Au NPs (Hao et al. 2020). First, CdS QDs nanostructure was synthesized. 20 mmol L^{-1} $CdCl_2$ and 20 mmol L^{-1} MPA were mixed, and the pH of the solution was adjusted to 11 using 1 mol L^{-1} NaOH. Afterward, 20 mmol L^{-1} thioacetamide was added, and the mixture was stirred for 30 min at room temperature; in sequence, the temperature was enhanced to 80 °C and kept for 10 h. Finally, the purification of CdS QDs nanostructure was followed by applying deionized water for 12 h at room temperature. In another procedure, Au-luminol-DNA2 Probe was produced. Initially, Au-luminol solution was prepared and then mixed with a thiol-functionalized aptamer sequence (DNA 2: 5′-Cy5-TATCCAGCTTATTCAATTTTTTTT–$(CH_2)_6$-SH-3′). After 12 h, Au-S covalent bond was established between the Au and thiol molecules, and a conjugated structure of Au-luminol-DNA2 Probe was achieved. In order to design the electrochemical biosensing platform, an ITO electrode was used as the signal transducer and modified with PANI via an electropolymerization procedure(−0.2 V to +0.8 V at 100 mV s^{-1}). At the next step, the ITO-PANI was modified with Au NP colloid (Fig. 38.4). Subsequently, a peptide sequence (DKDKDKDPPPPC) was

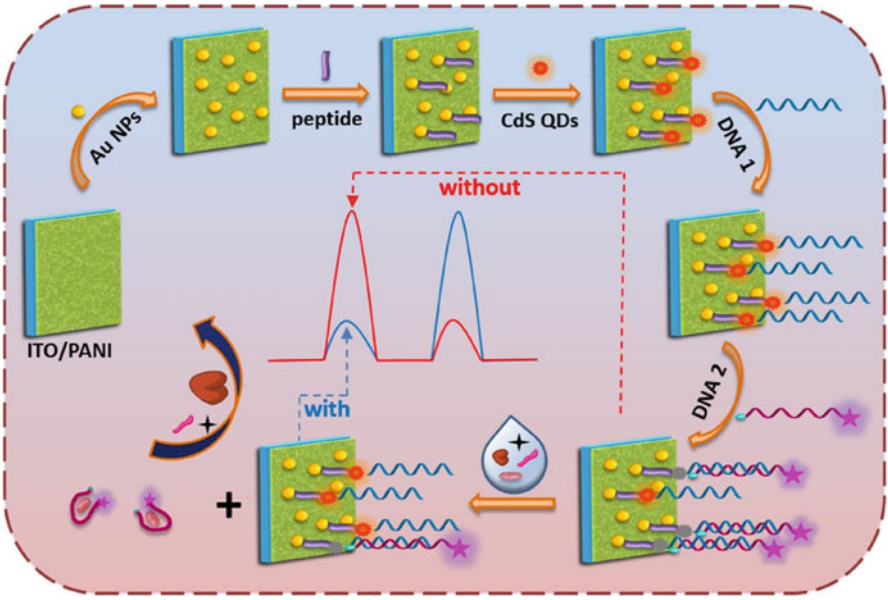

Fig. 38.4 An ECL peptide-aptamer biosensor for detection of CEA by applying the modified ITO electrode with PANI and Au NPs. (Reproduced with permission from Hao et al. (2020))

immobilized on the surface of ITO-PANI-Au NPs. The interaction between the peptide sequence and ITO-PANI-Au NPs occurred through the Au-S covalent bond. At the next step, the carboxyl group of the prepared CdS QDs nanostructure was activated by EDC/NHS, and then this nanostructure was coated on the surface of ITO-PANI-Au NPs-peptide (Fig. 38.4). At this point, an amine-functionalized aptamer sequence (DNA1: 5′-AATTGAATAAGCACCCCCTTTTTT-$(CH_2)_6$-NH_2-3′) was immobilized on the surface of ITO-PANI-Au NPs-peptide-CdS QDs nanostructure and could create the amide bond with CdS QDs nanostructure molecules. As the final step, enough amount of the prepared Au-luminol-DNA2 Probe was dropped on the surface of the signal transducer, and hybridization could be established between DNA1 and DNA2 strands. The prepared biosensor was applied for the determination of the various concentrations of CEA. In the designed biosensor, the CdS QDs nanostructure was applied as the cathode ECL emitter, and the Au-luminol-DNA2 Probe (containing Cy5 as the fluorophore agent) was as the anode ECL emitter. In the absence of the analyte, the negative potential related to the ECL signal of CdS QDs nanostructure was quenched, and the positive potential related to the ECL signal of the Au-luminol-DNA2 probe remained. However, in the presence of the analyte, the affinity between the DNA1 and CEA was intense to break the hybridization between DNA1 and DNA2. This event led to the decrement in the positive potential of the Au-luminol-DNA2 probe and an enhancement in negative potential related to the ECL signal of CdS QDs nanostructure. The ratio between ECL output responses provided a quantitative method for the detection of

this cancer biomarker. This biosensor could detect CEA in a linear range up to 100 ng mL^{-1} and with an LOD of about 0.13 pg mL^{-1}.

In Table 38.2, comprehensive details for nano and peptide-based biosensors designed to diagnose various diseases have been provided.

4 Applications of the Electrochemical Nanoaptasensors in the Early Diagnosis of Diseases

An aptasensor based on electrochemiluminescence (ECL) was developed to determine various concentrations of TnI by using a modified GCE with CdS QDs (Kitte et al. 2021). In this research, two nanostructures were applied. First, CdS QDs (medium size: 5 nm) were synthesized from a mixture of 0.017 mol L^{-1} Cd $(NO_3)_2{\cdot}4H_2O$ and 0.082 mol L^{-1} $Na_2S{\cdot}9H_2O$. In the second procedure, Au nanoparticles (Au NPs) (medium size: 5 nm) were synthesized by mixing 0.1 mol L^{-1} $NaBH_4$ and 0.25 mmol L^{-1} $HAuCl_4$ in a solution containing HCl/HNO_3 (3:1). A conjugated structure was obtained at the next step by mixing a defined concentration of (5′-CGCATGCCAAACGTTGCCTCATAGTTCCCTCCCCGTGTCC-3′)-a thiol-functionalized aptamer-and Au NPs. In order to design this aptasensing platform, a GCE was chosen as the signal transducer, and its surface was modified with CdS QDs nanostructure. Subsequently, to establish the carboxyl groups on the surface of this signal transducer, a solution containing 3-mercaptopropionic acid (MPA), 0.1 mol L^{-1} NaCl, and 0.1 mol L^{-1} PBS (pH 7.4) was used. Then, the obtained carboxyl groups were activated by immersing the electrode in 25 mmol L^{-1} 1-ethyl-3-(3-dimethylaminopropyl)-carbodiimide hydrochloride/N-hydroxy-succinimide (EDC/NHS) (1:1) solution. Afterward, (5′-CGTGCAGTACGCCAACCTTTCT CATGCGCTGCCCCTCTTA-3′) an amine-functionalized aptamer was immobilized on the surface of the prepared GCE, and nonspecific binding sites were blocked by mercaptohexanol (MCH). Then TnI as the analyte was added on the surface of the signal-transducer. Finally, the conjugated aptamer-Au NPs were added, and consequently, a sandwich structure was established (Au NPs-aptamer/TnI/aptamer/CdS QDs nanostructure/GCE). The electrochemical measurements were followed in a solution containing $[Fe(CN)_6]^{3-/4-}$ as the redox signal marker and in a three-electrode system, whereas the modified GCE, platinum, and Ag/AgCl electrodes were applied as the working, counter, and reference, respectively. The ECL assays were performed in the presence of 0.05 M $S_2O_8{}^{2-}$ as the coreactant agent. The presence of TnI as the analyte was led to develop the sandwich structure based on the found affinity between aptamers strands and analyte molecules, while the used nanostructures created an optimum electron transfer rate. This event provided ECL signals at the maximum value, and this event had a direct relation along with enhancement of the concentrations of the analyte. According to the authors, the linear detection range for this TnI aptasensor was situated between 1 fg mL^{-1} to 10 ng mL^{-1}, and the obtained LOD was 0.75 fg mL^{-1}.

Table 38.2 The features and details about applied components in recent developed electrochemical nano and peptide-based biosensors for diagnosis of diseases

Analyte	Transducer	Peptide	Functional group interacted with the peptide sequence	Nanomaterial(s)	Redox marker	Detection technique	Detection range	LOD	Ref.
Botulinum neurotoxin serotype A and C	Paper-based electrode	CLYRIDEANQRATLM	Thiol	Au NPs	$[Fe(CN)_6]^{3-/4-}$	SWV	Up to 1 nmol L^{-1}	10 pmol L^{-1}	Caratelli et al. (2021)
Candida yeasts (*C. krusei*, *C. glabrata*, *C. albicans*, and *C. tropicalis*)	GE	Clavanin A: VFQFLGKIIHHVGNFV HGFSHVF	Nonpolar amino acid residues (FLPII)	TiO_2 NPs	$[Fe(CN)_6]^{3-}$	EIS	10^1–10^6 CFU mL^{-1}	2–3 CFU mL^{-1}	Ribeiro et al. (2021)
E. coli O157:H7	SPCE	QKVNIDELGNAIPS GVLKDD	Thiol	Au NPs	$[Fe(CN)_6]^{3-/4-}$	EIS	Up to 500 CFU mL^{-1}	2 CFU mL^{-1}	Ropero-Vega et al. (2021)
AFP	GCE	CPPPPEKEKEKEK	NH_2	PANI	$[Fe(CN)_6]^{3-/4-}$	DPV	0.1 fg mL^{-1}–1 ng mL^{-1}	0.03 fg mL^{-1}	Zhao et al. (2021)
miRNA-192	Pencil graphite electrode (PGE)	FF	–[a]	GO	$[Fe(CN)_6]^{3-/4-}$	EIS	10 fmol L^{-1}–1 n mol L^{-1}	8 fmol L^{-1}	Bolat et al. (2021)
PSA	GCE	CGGGGMERCPIKMFY NLGSPYMNI	–[a]	Au@PDA@BCN nanocomposite/ AuPt@MnO_2@COF nanocomposite	$[Fe(CN)_6]^{3-/4-}$	DPV	0.00005–10 ng mL^{-1}	16.7 fg mL^{-1}	Zheng et al. (2021)
Matrix metalloproteinase 2 (MMP-2)	GE	FGPLGVRGKGGC/ FGGGASLWWSEKL	Cucurbit[8]uril (CB[8])	Ag NPs	$[Fe(CN)_6]^{3-/4-}$	SWV	0.5 pg mL^{-1}–50 ng mL^{-1}	0.12 pg mL^{-1}	Cheng et al. (2021)
Tumor exosomes	GCE	FNFRLKAGAKI RFGRGC	Thiol	Au NFs/Au NPs@g-C_3N_4 nanocomposite	$[Fe(CN)_6]^{3-/4-}$	ECL	1×10^2–1×10^7 particles μL^{-1}	39 particles μL^{-1}	Liu et al. (2021)

Dopamine	GCE	FEKF	Fluorene methoxycarbonyl (Fmoc)	Au NPs	Fluorine methoxycarbonyl (Fmoc)	DPV	0.1–10 μmol L^{-1}	21 nmol L^{-1}	Wang et al. (2021c)
Human chorionic gonadotrophin (hCG)	ITO	PPLRINRHILTR/ EKEKEKEPPPPC	NH_2	Au NPs	$[Fe(CN)_6]^{3-/4-}$	PEC	0.5–1000 mIU mL^{-1}	0.19 mIU mL^{-1}	Gu et al. (2021)
TnI	Mercury film modified screen-printed electrode	FYSHSFHENWPS/ GGGAFYSHSFHENWPSK	Biotin	QDs/magnetic beads	–[b]	DPV	0.001–100 ng mL^{-1}	0.42 pg mL^{-1}	Han et al. (2021a)
Trypsin	GCE	HWRGWVC	–[a]	Au NPs/Ag@CeO_2 NPs	$S_2O_8^{2-}/SO_4^{\cdot-}$	ECL	10 fg mL^{-1}–100 ng mL^{-1}	3.46 fg mL^{-1}	Song et al. (2021)
Protein kinase A	ITO	LRRASLGGGGC	Thiol	Au NPs/ZrO_2-CdS octahedral nanocomposite	$[Fe(CN)_6]^{3-/4-}$	PEC	0.001–100 U mL^{-1}	0.00035 U mL^{-1}	Xiao et al. (2021)
Rituximab	GE	CGSGSGSWPRWLEN	–[a]	Au NPs	$[Fe(CN)_6]^{3-/4-}$	EIS	0.1–50 μg mL^{-1}	35.26 ng mL^{-1}	Huang et al. (2021)
Immunoglobulin G (IgG)	GCE	CPPPPEK(HWRGWVA) EKEKE/CPPPPEK EKEKE HWRGWVA	Thiol	Au NPs	$[Fe(CN)_6]^{3-/4-}$	DPV	100 pg mL^{-1}–10 μg mL^{-1}	32 pg mL^{-1}	Chen et al. (2021b)
Antibody of rheumatoid arthritis	Screen-printed polycarbonate electrode	Inter-alpha-trypsin inhibitor-3 $(ITIH3)^{542–556}$	Thiol	Au NPs	$[Fe(CN)_6]^{3-/4-}$	EIS	0.25–1 mmol L^{-1}	–[c]	Lin et al. (2022)
Human epidermal growth factor receptor 2 (HER2)	GCE	FEKF	Fluorine methoxycarbonyl group (Fmoc)	Nanofibrous network structure	Fmoc/$[Fe(CN)_6]^{3-/4-}$	DPV	0.1 ng mL^{-1}–1 μg mL^{-1}	45 pg mL^{-1}	Tao et al. (2021a)
CEA	ITO	DKDKDKDPPPPC	Thiol	CdS QDs/Au NPs	$[Fe(CN)_6]^{3-/4-}$	ECL	Up to 100 ng mL^{-1}	0.13 pg mL^{-1}	Hao et al. (2020)

[a]The functional group interacted with the peptide sequence not reported
[b]The redox marker not reported
[c]The LOD not reported

In another investigation, a photoelectrochemical (PEC) aptasensor was developed for early detection of PSA by applying ZnO NA-CdS nanocomposite and iodide-doped bismuth oxychloride flower-array ($I_{0.2}$:$BiOCI_{0.8}$) as the photocathode agent (Feng et al. 2021). The zinc oxide nanorod array (ZnO NA) was initially synthesized by preparing a mixture containing 0.02 mol L^{-1} $Zn(NO_3)_2{\cdot}6H_2O$, 0.03 mol L^{-1} NaOH, and methanol. This mixture was heated several times at 60 °C to dry on the reference/counter microelectrodes. Afterward, to do the calcination process, the temperature of the mixture was reached to 350 °C and kept for 30 min. Then, the obtained ZnO seed was mixed with a solution containing 0.05 mol L^{-1} Zn $(NO_3)_2{\cdot}6H_2O$ and 0.05 mol L^{-1} hexamethylenetetramine, and the obtained mixture was kept at 90 °C for 6 h. Finally, the CdS QDs were added (drop by drop), producing ZnO NA-CdS nanocomposite. This nanocomposite was used as the photoanode. The indium tin oxide (ITO) equipped with poly (dimethylsiloxane) (PDMS) microelectrode channels was applied as the working electrode, and then $I_{0.2}$:$BiOCI_{0.8}$ as a photocathode was synthesized on its surface with the following procedure. A mixture of NaCI and KI was prepared and dissolved in the deionized water (solution 1), and $Bi(NO_3)_3{\cdot}5H_2O$ was dissolved in glycol (solution 2). Afterward, solution 1 and solution 2 were added on the surface of the working electrode in sequence. Then, the chitosan solution containing acetic acid and glutaraldehyde was added on the surface of the modified working electrode with $I_{0.2}$:$BiOCI_{0.8}$ to provide the immobilization capability of the biorecognition element. At the next step, an amine-functionalized aptamer sequence (5′-NH_2-C_6-AATTAAAGCTCGCCATCAAATAGC-3′) as the biorecognition element was added on the surface of the signal transducer, and the BSA solution was also applied to prevent unwanted immobilization of the aptamer strands. Finally, the prepared aptasensor was used for the detection of various concentrations of PSA based on the variations of the cathodic photocurrents in the presence of luminol as the chemiluminescence agent. This aptasensor reported a linear detection range for PSA from 50 fg mL^{-1} to 50 ng mL^{-1}, and the reported LOD was about 25.8 fg mL^{-1}.

In another research, a CEA aptasensor was developed by modifying a GCE with polydopamine (PDA)@graphene (Gr) (Zhang et al. 2021a). Initially, PDA@Gr nanocomposite was synthesized; GO was first synthesized from graphite powder based on the Hummers' method. Then, 100 μL ammonia was mixed with 1 mg mL^{-1} GO and stirred. Afterward, 1 mg mL^{-1} dopamine, hydrazine hydrate, and deionized water were also added to the GO mixture. The obtained mixture was finally stirred at room temperature for 20 min and subsequently was kept at 60 °C for 4 h to achieve the final PDA@Gr nanocomposite. In another procedure, PDA@Gr-Pd-Pt nanodendrites (NDs) nanostructure was synthesized; first, the concentration of 0.50 mg mL^{-1} PDA@Gr nanocomposite was prepared and then mixed with a defined amount of PDDA and 10 mg mL^{-1} K_2PdCl_4. Afterward, 20 mmol L^{-1} $NaBH_4$ was added to the above mixture and stirred while it was kept at 25 °C for 30 min. At this step, PDA@Gr-PdNPs nanostructure was attained. Finally, to synthesize PDA@Gr-Pd-PtNDs nanostructure, a considered amount of PDDA and ascorbic acid was added to PDA@Gr-PdNPs nanostructure and then stirred. The temperature was raised and fixed when attained at 90 °C. At this moment, H_2PtCl_6

was added to the final mixture, and after 180 min, PDA@Gr-Pd-PtNDs, the desired nanostructure, was obtained. In another procedure, an amine-functionalized aptamer sequence (aptamer 2: 5′-AGGGGGTGAAGGGATACCC-3′) was applied and mixed with PDA@Gr-Pd-PtNDs nanostructure, and the conjugation (covalent binding: Pd-NH and Pt-NH) process was followed by stirring for 180 min. Finally, 0.50 mg mL^{-1} hemin was added to the final mixture, and the product was stirred for 60 min at 4 °C; in sequence, the aptamer 2-hemin-PDA@Gr/Pd-PtNDs structure was obtained. In order to provide the aptasensing structure, a GCE was elected as the working electrode and modified with PDA@Gr nanocomposite. Afterward, an aptamer sequence (aptamer 1: 5′-ATACCAGCTTATTCAATT-3′) as a part of the biorecognition element was immobilized on the surface of GCE-PDA@Gr. Subsequently, the analyte was dropped on the surface of GCE-PDA@Gr-aptamer 1 and could be bound with the aptamer 1 from one side. In addition, the conjugated aptamer 2 with PDA@Gr/Pd-PtNDs nanostructure was immobilized on the surface of the electrode and created a sandwich platform where the analyte was located between two aptamer sequences (GCE-PDA@Gr-aptamer 1-CEA-aptamer 2-PDA@Gr/Pd-PtNDs). The electrochemical assays were followed by DPV techniques and in the presence of hydroquinone (HQ) as the redox marker and in a three-electrode system (GCE: working; platinum: counter; saturated calomel electrode: reference). During the electrochemical assays, the maximum electron transfer rate was found in the absence of the analyte. In the presence of the analyte, due to the existing affinity between the aptamer strands (aptamer 1 and aptamer 2) and the analyte (CEA), the creation sandwich structure (aptamer 1-CEA-aptamer 2) reduced the electron transfer rate proportionally. The reduction of DPVs peak currents depended on concentrations of CEA. The higher concentration of the analyte created the bigger accumulation of bound aptamers-analyte units resulting in greater obstruction for electron transfer. This signal-off aptasensor detected the CEA in a linear range from 50 pg mL^{-1} to 1 μg mL^{-1}, and the reported LOD was about 6.3 pg mL^{-1}. In Table 38.3, details for electrochemical nanoaptasensors designed to diagnose various diseases have been provided.

5 A Summary and a Viewpoint About Electrochemical Nanobiosensors: Construction and Diagnosis of Diseases

In previous sections, the different kinds of electrochemical nanobiosensors applied for different diseases were examined. Details of these sensors are presented in Tables 38.1, 38.2, and 38.3 including information about the nanomaterials used. The biorecognition elements used in the structure of biosensors: antibodies, aptamers, and peptides, were considered to build Tables 38.1, 38.2, and 38.3. The performance of this kind of electrode is determined by the influence of various factors such as the type of nanostructure used to modify the electrode surface, the technique used in electrochemical assays, the type of redox marker, and the type of analyte. Indeed, when calibrating the biosensor platform, the optimal signal transducer should be selected. Different signal transducers such as GCE, gold electrode

Table 38.3 The features and details about applied components in recent developed electrochemical nanoaptasensors for diagnosis of diseases

Analyte	Transducer	Aptamer sequence	Functional group interacted with aptamer	Nanomaterial (s)	Redox marker	Detection technique (s)	Detection range	LOD	Ref.
Amyloid beta (Aβ)	ITO	5′-GCCTGTGTTGG GGCGGGTGCG-3′	NH_2	MoS_2 QDs@Cu NWs/CuO/g-C_3N_4 nanosheets	4-chloro-1-naphthol (4-CN)	PEC	10 fmol L^{-1}–0.5 μmol L^{-1}	5.79 fmol L^{-1}	Zhang et al. (2021b)
Tau-381 protein	CPE	5′-GCGGAGCGT GGCAGG-3′	Thiol	Au NPs-$MoSe_2$ NSs nanocomposite	$[Fe(CN)_6]^{3-/4-}$	PEC	0.5 fM–1.0 nmol L^{-1}	0.3 fmol L^{-1}	Hun and Kong (2021)
Dopamine	GCE	5′-GTCTCTGTGT GCGCCAGAGAAC ACTGGGGCAGATAT GGGCCAGCACAGA-ATGAGGCCC-3′	Thiol	rGO/Au NPs	$[Fe(CN)_6]^{3-/4-}$	DPV	5×10^{-8}–1×10^{-5} mol L^{-1}	4.7×10^{-8} mol L^{-1}	Shen and Kan (2021)
Glycated albumin	SPCE	5′-TGCGGTTCG TGCGGTTG TAGTAC-3′	Biotin	GO-Pb nanocomposite	$[Fe(CN)_6]^{3-/4-}$	SWV	0.005–10 μg mL^{-1}	0.77 ng mL^{-1}	Putnin et al. (2021)
Adenosine triphosphate (ATP)	GCE	5′-TGGAAGGAG GCGTTATGAG GGGGTCCA-3′	NH_2	Mesoporous Fe_3O_4@Cu@Cu_2O	[Ru $(bpy)_2(dppz)]^{2+}$	ECL	0.5–2500 nmol L^{-1}	0.17 nmol L^{-1}	Qing et al. (2021)
Thrombin	ITO	5′-GGTTGGT GTGGTTGG-3′/5′-AGTCCGTG GTAGGGCAGG TTGGGGTGACT-3′	Thiol/NH_2	Silver nanowires (Ag NWs)-particles (PCs)/Pt-zinc ferrite ($ZnFe_2O_4$)	$[Fe(CN)_6]^{3-/4-}$	Chronoamperometry (CA)	0.05 pmol L^{-1}–35 nmol L^{-1}	0.016 pmol L^{-1}	Zhang et al. (2021c)
α-synuclein	GCE	5′-TTTTTGGTG GCTGGAGGGGG CGCGAACG-3′	NH_2	Au nanostars (Au NSs)	$[Fe(CN)_6]^{3-/4-}$	EIS	0.10 amol L^{-1}–10 fmol L^{-1}	0.07 amol L^{-1}	Tao et al. (2021b)
TnI	SPCE	5′-NH_2-$(CH_2)_6$-CGTGCAGTAC GCCAACCTTT CTCATGCGCTG CCCCTCTTA-3′	NH_2	GO	HQ	Amperometry	1 pg mL^{-1}–1 μg mL^{-1}	0.6 pg mL^{-1}	Villalonga et al. (2021)

p24-HIV protein	SPE	p24 ssDNA aptamer	NH_2	Graphene QDs	$[Fe(CN)_6]^{3-/4-}$	CV	0.93 ng mL^{-1}–93 μg mL^{-1}	51.7 pg mL^{-1}	Gogola et al. (2021)
SARS-CoV-2 S-protein	SPCE	5′-CAGCACCGACC TTGTGCTTTGGG AGTGCTGGTCCAA GGGCGTTAATG GACA-3′	Thiol	Au NPs	$[Fe(CN)_6]^{3-/4-}$	EIS	10 pmol L^{-1}–25 nmol L^{-1}	1.30 pmol L^{-1}	Abrego-Martinez et al. (2022)
17β-Estradiol (E2)	GCE/laser-scribed graphene electrode (LSGE)	5′-NH_2-AAGGGATGCC GTTTGGG-3′/5′-CCCAAGTTCGGC ATAGTG-SH-3′/5′ -AAGCTTGGGCCATG CCCAGGAAGGACCC AAACGG-3′/5′-CCGTTTGGG TCCTTCCTGGGCA TGGCCCAAGCTT-3′	NH_2/thiol	Graphene/Au NPs	$[Fe(CN)_6]^{3-/4-}$	DPV	1×10^{-13}–1×10^{-9} mol L^{-1}	63.1 fmol L^{-1}	Chang et al. (2021)
TnI	GCE	5′-CGTGCAGTACGCCAACC TTTCTCATGCGCTG CCCCTCTTA-3′/5′-CGCATGCCAAACGT TGCCTCATAGTT CCCTCCCCG TGTCC-3′	Carboxyl/thiol	CdS QDs/Au NPs	$[Fe(CN)_6]^{3-/4-}$	ECL	1 fg mL^{-1}–10 ng mL^{-1}	0.75 fg mL^{-1}	Kitte et al. (2021)
TnI	GE	5′-CGTGCAGTAC GCCAACCTTT CTCATGCGCTG CCCCTCTTA-3′	–[a]	Nanodiamonds (NDs) and hydrogen-substituted graphdiyne (HsGDY) HsGDY@NDs	$[Fe(CN)_6]^{3-/4-}$	EIS	0.00001–100 ng mL^{-1}	6.29 fg mL^{-1}	Wang et al. (2021a)
SARS-CoV-2 nucleocapsid protein (2019-nCoV-NP)	GE	5′-GCTGGATGTC GCTTACGACAATAT TCCTTAGGGGCACCG CTACATTGACA CATCCAGC-3′/5′ -GCTGGATGTTGACC	Thiol	MOFs NH_2–MIL-53 NPs/Au@Pt NPs	HQ	DPV	0.025–50 ng mL^{-1}	8.33 pg mL^{-1}	Tian et al. (2021b)

(continued)

Table 38.3 (continued)

Analyte	Transducer	Aptamer sequence	Functional group interacted with aptamer	Nanomaterial (s)	Redox marker	Detection technique (s)	Detection range	LOD	Ref.
		TTTACAGATCGGA TTCTGTGGGGCG TTAAACTGACA CATCCAGC-3′							
MCF-7 cancer cells	GCE	5′-NH_2-TTTGGTGGT GGTGGTTGTG GTGGTGGTG G-3′	NH_2	rGO-chitosan-Au NPs nanocomposite	$[Fe(CN)_6]^{3-/4-}$	EIS	1×10^1–1×10^6 cells mL^{-1}	4 cells mL^{-1}	Shafiei et al. (2021)
Her-2	Laser-scribed graphene (LSG)-based electrodes	5′-AACCGCCCAAATCC CTAAGAGTCTGC ACTTGTCATTTTG TATATGTATTTGGTT TTTGGCTCTCAC AGACACACTAC ACACGCACA-3′	Thiol	Au NPs	$[Fe(CN)_6]^{3-/4-}$	SWV	0.1–200 ng mL^{-1}	0.008 ng mL^{-1}	Rauf et al. (2021a)
TnI	LSG-based electrodes	5′-CGTGCAGTACGCC AACCT TTCTCAT GCG CTGCCC CTCTTA-3′	Thiol	Zinc ferrite NPs ($ZnFe_2O_4$ NPs)	$[Fe(CN)_6]^{3-/4-}$	SWV	0.001–200 ng mL^{-1}	0.001 ng mL^{-1}	Rauf et al. (2021b)
TnI	GCE	5′-CGTGCAGTACG CCAACCTTTCT CATGCGCTGC CCCTCTTA-3′	–[a]	Cu NWs/MoS_2/rGO nanocomposite	$[Fe(CN)_6]^{3-/4-}$	DPV	5×10^{-13}–1×10^{-10} g mL^{-1}	1×10^{-13} g mL^{-1}	Han et al. (2021b)
SARS-Cov-2 receptor-binding domain (RBD)	ITO	5′-NH_2-$(CH_2)_6$-CAGCACCGA CCTTGTGCT TTGGGAGTG CTGGTCCAAGGG CGTTAATG GACA-3′	NH_2	gC_3N_4 CdS QDs	$[Fe(CN)_6]^{3-/4-}$	PEC	0.5–32 nmol L^{-1}	0.12 nmol L^{-1}	Amouzadeh Tabrizi et al. (2021)

CEA	GCE	5′-ATACCAGCTT ATTCAATT-3′/5′ -AGGGGGTGA AGGGATACC C-3′	NH_2	PDA@Gr/Pd-Pt NDs	HQ/$[Fe(CN)_6]^{3-/4-}$	DPV	50 pg mL^{-1}– 1 μg mL^{-1}	6.3 pg mL^{-1}	Zhang et al. (2021a)
MUC1	GCE	5′-NH_2-TTTTTGCAGTT GATCCTTTGGAT ACCCTGG-3′	NH_2	$Ru(bpy)_3^{2+}$@SiO_2 NPs	$[Fe(CN)_6]^{3-/4-}$	ECL	7.53–753 μg mL^{-1}	0.83 μg mL^{-1}	Hu et al. (2021)
Tumor necrosis factor α (TNF-α)	GE	5′-biotin-GCGGCCGATAAG GTCTTTCCAAGCGA ACGAATTGAAC CGC-3′	Biotin	CeO_2@Au NRs	$[Fe(CN)_6]^{3-/4-}$	DPV	2– 2 × 10^6 pg mL^{-1}	0.6 pg mL^{-1}	Ding et al. (2021)
Epithelial sodium channel (ENaC)	SPCE	5′-CGGTGAGGG TCGGGTCCA GTAGGCCTA CTGTTGAGT AGTGGGCTCC-3′	NH_2	CeO_2 NPs	$[Fe(CN)_6]^{3-/4-}$	DPV	0.05–3.0 ng mL^{-1}	0.012 ng mL^{-1}	Hartati et al. (2021)
PSA	ITO	5′-AATTAAAGC TCGCCATCAAA TAGC-3′	NH_2	CdS/ZnO NA	$[Fe(CN)_6]^{3-/4-}$	PEC	50 fg mL^{-1}– 50 ng mL^{-1}	25.8 fg mL^{-1}	Feng et al. (2021)

[a]The functional group interacted with the aptamer sequence not reported

(GE), ITO, screen-printed electrodes, and so on were applied in the sensors gathered in Tables 38.1, 38.2, and 38.3. Each of these biomolecules has advantages and disadvantages, the priorities of which have varied according to the goals of the researchers. One of the essential points that should be considered in using the biorecognition elements is considering the functional groups used in interaction with these biomolecules. These functional groups are used to adapt successful interactions with the target surfaces. The stability and compatibility of these functional groups with the biorecognition elements play an important role in the sensitivity, stability, reproducibility, and regeneration of biosensors. The most important functional groups used in the biorecognition elements structure were thiol and amine. Usually, the thiol group is important to establish successful interactions with gold. The amine functional group is more suitable for interaction with carbon-based surfaces. The biorecognition elements are immobilized on surfaces in two general ways. In the first case, these biomolecules are fixed directly on the surface of the signal transducer (bare or modified surface with nanostructures). In the second case, several types of biorecognition elements are used in the structure of biosensors. In this case, the simultaneous use of antibody-aptamer, antibody-peptide, aptamer-peptide, antibody-antibody, peptide-peptide, and aptamer-aptamer can be mentioned. In some cases, one of the mentioned units, including antibodies, aptamers, or peptides, is not immobilized on the surface of the signal transducer directly and interacts with the other components of the biorecognition element. The analytes considered in the investigated electrochemical nanobiosensors in most cases include markers of diseases with high importance in the early diagnosis such as cancers, MI, etc., which early diagnosis can prevent severe mortality and also pave the way for successful and low-cost treatments. Various diagnostic techniques were used in the studied electrochemical nanobiosensors, the most important of which include DPV, EIS, SWV, ECL, and PEC. Other important information of the studied biosensors such as detection range, LOD, and redox markers used has also been included in Tables 38.1, 38.2, and 38.3.

6 Final Remarks

Nanobiosensors have opened new roads for optimal disease diagnosis. In this chapter, we evaluated the application of electrochemical nanobiosensors in the diagnosis of several critical diseases. The purpose of using nanomaterials in the structure of biosensors is to provide more reliable diagnoses. In fact, the nanomaterials used have improved the reactivity and sensitivity of biosensors due to their increased surface-to-volume ratio. In addition, the nanostructures used as the biosensor components have created more stable bonds between the various biosensor components due to their specific morphologies. Nanomaterials used in the structure of electrochemical biosensors have been used both individually and in combination as nanocomposite structures.

Acknowledgments This chapter was supported by São Paulo State Foundation for Research – FAPESP (Fellowship 2019/27021-4 and projects 2014/50867-3 and 2017/13137-5) and the National Council for Research – CNPq (process 311847-2018-8).

References

Abrego-Martinez JC, Jafari M, Chergui S, Pavel C, Che D, Siaj M (2022) Aptamer-based electrochemical biosensor for rapid detection of SARS-CoV-2: nanoscale electrode-aptamer-SARS-CoV-2 imaging by photo-induced force microscopy. Biosens Bioelectron 195:113595

Al-Kazzaz FF, Dr SAM (2015) Molecular characterization of carcinoembryonic antigen (CEA) in some colorectal tumors. CreateSpace Independent Publishing Platform, Scotts Valley

Al-Mudhaffar SA, Dr SAM (2017) Protein engineering of of carcinoembryonic antigen and their receptors: protein engineering. CreateSpace Independent Publishing Platform, Scotts Valley

Amouzadeh Tabrizi M, Nazari L, Acedo P (2021) A photo-electrochemical aptasensor for the determination of severe acute respiratory syndrome coronavirus 2 receptor-binding domain by using graphitic carbon nitride-cadmium sulfide quantum dots nanocomposite. Sensors Actuators B Chem 345:130377

Aydin EB, Aydin M, Sezgintürk MK (2021a) Fabrication of electrochemical immunosensor based on acid-substituted poly(pyrrole) polymer modified disposable ITO electrode for sensitive detection of CCR4 cancer biomarker in human serum. Talanta 222:121487

Aydin EB, Aydin M, Sezgintürk MK (2021b) A novel electrochemical immunosensor based on acetylene black/epoxy-substituted-polypyrrole polymer composite for the highly sensitive and selective detection of interleukin 6. Talanta 222:121596

Bakshi S, Mehta S, Kumeria T, Shiddiky MJ, Popat A, Choudhury S, Bose S, Nayak R (2021) Rapid fabrication of homogeneously distributed hyper-branched gold nanostructured electrode based electrochemical immunosensor for detection of protein biomarkers. Sensors Actuators B Chem 326:128803

Bhatnagar I, Mahato K, Ealla KKR, Asthana A, Chandra P (2018) Chitosan stabilized gold nanoparticle mediated self-assembled gliP nanobiosensor for diagnosis of invasive Aspergillosis. Int J Biol Macromol 110:449–456

Boeri L, Capogrosso P, Cazzaniga W, Ventimiglia E, Pozzi E, Belladelli F, Schifano N, Candela L, Alfano M, Pederzoli F (2021) Infertile men have higher prostate-specific antigen values than fertile individuals of comparable age. Eur Urol 79:234–240

Bolat G, Akbal Vural O, Tugce Yaman Y, Abaci S (2021) Label-free impedimetric miRNA-192 genosensor platform using graphene oxide decorated peptide nanotubes composite. Microchem J 166:106218

Boonkaew S, Jang I, Noviana E, Siangproh W, Chailapakul O, Henry CS (2021) Electrochemical paper-based analytical device for multiplexed, point-of-care detection of cardiovascular disease biomarkers. Sensors Actuators B Chem 330:129336

Butler SS, Muralidhar V, Zhao SG, Sanford NN, Franco I, Fullerton ZH, Chavez J, D'Amico AV, Feng FY, Rebbeck TR (2020) Prostate cancer incidence across stage, NCCN risk groups, and age before and after USPSTF Grade D recommendations against prostate-specific antigen screening in 2012. Cancer 126:717–724

Caratelli V, Fillo S, D'Amore N, Rossetto O, Pirazzini M, Moccia M, Avitabile C, Moscone D, Lista F, Arduini F (2021) Paper-based electrochemical peptide sensor for on-site detection of botulinum neurotoxin serotype A and C. Biosens Bioelectron 183:113210

Cen S-Y, Ge X-Y, Chen Y, Wang A-J, Feng J-J (2021) Label-free electrochemical immunosensor for ultrasensitive determination of cardiac troponin I based on porous fluffy-like AuPtPd trimetallic alloyed nanodendrites. Microchem J 169:106568

Chandra P, Koh WCA, Noh H-B, Shim Y-B (2012) In vitro monitoring of i-NOS concentrations with an immunosensor: the inhibitory effect of endocrine disruptors on i-NOS release. Biosens Bioelectron 32:278–282

Chang Z, Zhu B, Liu J, Zhu X, Xu M, Travas-Sejdic J (2021) Electrochemical aptasensor for 17β-estradiol using disposable laser scribed graphene electrodes. Biosens Bioelectron 185:113247

Chapman AR, Adamson PD, Shah AS, Anand A, Strachan FE, Ferry AV, Ken Lee K, Berry C, Findlay I, Cruikshank A (2020) High-sensitivity cardiac troponin and the universal definition of myocardial infarction. Circulation 141:161–171

Chen G-C, Liu C-H, Wu W-C (2021a) Electrochemical immunosensor for serum parathyroid hormone using voltammetric techniques and a portable simulator. Anal Chim Acta 1143:84–92

Chen M, Song Z, Han R, Li Y, Luo X (2021b) Low fouling electrochemical biosensors based on designed Y-shaped peptides with antifouling and recognizing branches for the detection of IgG in human serum. Biosens Bioelectron 178:113016

Chen S, Xu L, Sheng K, Zhou Q, Dong B, Bai X, Lu G, Song H (2021c) A label-free electrochemical immunosensor based on facet-controlled Au nanorods/reduced graphene oxide composites for prostate specific antigen detection. Sensors Actuators B Chem 336:129748

Cheng W, Ma J, Kong D, Zhang Z, Khan A, Yi C, Hu K, Yi Y, Li J (2021) One step electrochemical detection for matrix metalloproteinase 2 based on anodic stripping of silver nanoparticles mediated by host-guest interactions. Sensors Actuators B Chem 330:129379

Choudhary M, Yadav P, Singh A, Kaur S, Ramirez-Vick J, Chandra P, Arora K, Singh SP (2016) CD59 targeted ultrasensitive electrochemical immunosensor for fast and noninvasive diagnosis of oral cancer. Electroanalysis 28:2565–2574

de Crevoisier R, Bayar MA, Pommier P, Muracciole X, Pêne F, Dudouet P, Latorzeff I, Beckendorf V, Bachaud J-M, Laplanche A (2018) Daily versus weekly prostate cancer image guided radiation therapy: phase 3 multicenter randomized trial. Int J Radiat Oncol Biol Phys 102:1420–1429

Ding Y, Zhang M, Li C, Xie B, Zhao G, Sun Y (2021) A reusable aptasensor based on the dual signal amplification of Ce@AuNRs-PAMAM-Fc and DNA walker for ultrasensitive detection of TNF-α. J Solid State Electrochem 26(1):e8

Fabiani L, Saroglia M, Galatà G, de Santis R, Fillo S, Luca V, Faggioni G, D'Amore N, Regalbuto E, Salvatori P, Terova G, Moscone D, Lista F, Arduini F (2021) Magnetic beads combined with carbon black-based screen-printed electrodes for COVID-19: a reliable and miniaturized electrochemical immunosensor for SARS-CoV-2 detection in saliva. Biosens Bioelectron 171:112686

Fadila AN, Rahaju AS, Tarmono T (2020) Relationship of prostate-specific antigen (PSA) and prostate volume in patients with biopsy proven benign prostatic hyperplasia (BPH). Qanun Med 4:171–177

Fan X, Deng D, Chen Z, Qi J, Li Y, Han B, Huan K, Luo L (2021) A sensitive amperometric immunosensor for the detection of carcinoembryonic antigen using $ZnMn_2O_4$@reduced graphene oxide composites as signal amplifier. Sensors Actuators B Chem 339:129852

Felix FS, Angnes L (2018) Electrochemical immunosensors – a powerful tool for analytical applications. Biosens Bioelectron 102:470–478

Feng J, Dai L, Ren X, Ma H, Wang X, Fan D, Wei Q, Wu R (2021) Self-powered cathodic photoelectrochemical aptasensor comprising a photocathode and a photoanode in microfluidic analysis systems. Anal Chem 93:7125–7132

Ge X-Y, Feng Y-G, Cen S-Y, Wang A-J, Mei L-P, Luo X, Feng J-J (2021) A label-free electrochemical immnunosensor based on signal magnification of oxygen reduction reaction catalyzed by uniform PtCo nanodendrites for highly sensitive detection of carbohydrate antigen 15-3. Anal Chim Acta 1176:338750

Gogola JL, Martins G, Gevaerd A, Blanes L, Cardoso J, Marchini FK, Banks CE, Bergamini MF, Marcolino-Junior LH (2021) Label-free aptasensor for p24-HIV protein detection based on graphene quantum dots as an electrochemical signal amplifier. Anal Chim Acta 1166:338548

Gooding JJ (2006) Nanoscale biosensors: significant advantages over larger devices? Small 2: 313–315

Gu S, Shi X-M, Zhang D, Fan G-C, Luo X (2021) Peptide-based photocathodic biosensors: integrating a recognition peptide with an antifouling peptide. Anal Chem 93:2706–2712

Han K, Li G, Tian L, Li L, Shi Y, Huang T, Li Y, Xu Q (2021a) Multifunctional peptide-oligonucleotide conjugate promoted sensitive electrochemical biosensing of cardiac troponin I. Biochem Eng J 174:108104

Han Y, Su X, Fan L, Liu Z, Guo Y (2021b) Electrochemical aptasensor for sensitive detection of cardiac troponin I based on CuNWs/MoS_2/rGO nanocomposite. Microchem J 169:106598

Hao Q, Wang L, Niu S, Ding C, Luo X (2020) Ratiometric electrogenerated chemiluminescence sensor based on a designed anti-fouling peptide for the detection of carcinoembryonic antigen. Anal Chim Acta 1136:134–140

Hartati YW, Komala DR, Hendrati D, Gaffar S, Hardianto A, Sofiatin Y, Bahti HH (2021) An aptasensor using ceria electrodeposited-screen-printed carbon electrode for detection of epithelial sodium channel protein as a hypertension biomarker. R Soc Open Sci 8:202040

Hassanipour S, Delam H, Arab-Zozani M, Abdzadeh E, Hosseini SA, Nikbakht H-A, Malakoutikhah M, Ashoobi MT, Fathalipour M, Salehiniya H (2020) Survival rate of prostate cancer in Asian countries: a systematic review and meta-analysis. Ann Glob Health 86:2

Heiat M, Negahdary M (2019) Sensitive diagnosis of alpha-fetoprotein by a label free nano-aptasensor designed by modified Au electrode with spindle-shaped gold nanostructure. Microchem J 148:456–466

Hu Z, Zhao B, Miao P, Hou X, Xing F, Chen Y, Feng L (2021) Three-way junction DNA based electrochemical biosensor for microRNAs detection with distinguishable locked nucleic acid recognition and redox cycling signal amplification. J Electroanal Chem 880:114861

Huang S, Tang R, Zhang T, Zhao J, Jiang Z, Wang Q (2021) Anti-fouling poly adenine coating combined with highly specific CD20 epitope mimetic peptide for rituximab detection in clinical patients' plasma. Biosens Bioelectron 171:112678

Hun X, Kong X (2021) An enzyme linked aptamer photoelectrochemical biosensor for Tau-381 protein using AuNPs/$MoSe_2$ as sensing material. J Pharm Biomed Anal 192:113666

Kalyani T, Sangili A, Nanda A, Prakash S, Kaushik A, Kumar Jana S (2021) Bio-nanocomposite based highly sensitive and label-free electrochemical immunosensor for endometriosis diagnostics application. Bioelectrochemistry 139:107740

Katrukha I (2013) Human cardiac troponin complex. Structure and functions. Biochemistry 78: 1447–1465

Kitte SA, Tafese T, Xu C, Saqib M, Li H, Jin Y (2021) Plasmon-enhanced quantum dots electrochemiluminescence aptasensor for selective and sensitive detection of cardiac troponin I. Talanta 221:121674

Lin C-Y, Nhat Nguyen UT, Hsieh H-Y, Tahara H, Chang Y-S, Wang B-Y, Gu B-C, Dai Y-H, Wu C-C, Tsai IJ, Fan Y-J (2022) Peptide-based electrochemical sensor with nanogold enhancement for detecting rheumatoid arthritis. Talanta 236:122886

Liu X, Wang Q, Chen J, Chen X, Yang W (2021) Ultrasensitive electrochemiluminescence biosensor for the detection of tumor exosomes based on peptide recognition and luminol-AuNPs@g-C_3N_4 nanoprobe signal amplification. Talanta 221:121379

Logozzi M, Angelini DF, Giuliani A, Mizzoni D, Di Raimo R, Maggi M, Gentilucci A, Marzio V, Salciccia S, Borsellino G (2019) Increased plasmatic levels of PSA-expressing exosomes distinguish prostate cancer patients from benign prostatic hyperplasia: a prospective study. Cancers 11:1449

Mahapatra S, Baranwal A, Purohit B, Roy S, Mahto SK, Chandra P (2020) Advanced biosensing methodologies for ultrasensitive detection of human coronaviruses. In: Diagnostic strategies for COVID-19 and other coronaviruses. Springer, Singapore

Mahato K, Kumar S, Srivastava A, Maurya PK, Singh R, Chandra P (2018) Chapter 14. Electrochemical immunosensors: fundamentals and applications in clinical diagnostics. In: Vashist SK, Luong JHT (eds) Handbook of immunoassay technologies. Academic Press, Cambridge, MA

Mahato K, Purohit B, Bhardwaj K, Jaiswal A, Chandra P (2019) Novel electrochemical biosensor for serotonin detection based on gold nanorattles decorated reduced graphene oxide in biological fluids and in vitro model. Biosens Bioelectron 142:111502

Mair J, Lindahl B, Hammarsten O, Müller C, Giannitsis E, Huber K, Möckel M, Plebani M, Thygesen K, Jaffe AS (2018) How is cardiac troponin released from injured myocardium? Eur Heart J Acute Cardiovasc Care 7:553–560

Martínez-Rojas F, Castañeda E, Armijo F (2021) Conducting polymer applied in a label-free electrochemical immunosensor for the detection prostate-specific antigen using its redox response as an analytical signal. J Electroanal Chem 880:114877

Morales MA, Halpern JM (2018) Guide to selecting a biorecognition element for biosensors. Bioconjug Chem 29:3231–3239

Negahdary M (2020a) Aptamers in nanostructure-based electrochemical biosensors for cardiac biomarkers and cancer biomarkers: a review. Biosens Bioelectron 152:112018

Negahdary M (2020b) Electrochemical aptasensors based on the gold nanostructures. Talanta 216:120999

Negahdary M, Heli H (2018) Applications of nanoflowers in biomedicine. Recent Pat Nanotechnol 12:22–33

Negahdary M, Heli H (2019a) An electrochemical troponin I peptisensor using a triangular icicle-like gold nanostructure. Biochem Eng J 151:107326

Negahdary M, Heli H (2019b) An ultrasensitive electrochemical aptasensor for early diagnosis of Alzheimer's disease, using a fern leaves-like gold nanostructure. Talanta 198:510–517

Negahdary M, Behjati-Ardakani M, Sattarahmady N, Yadegari H, Heli H (2017) Electrochemical aptasensing of human cardiac troponin I based on an array of gold nanodumbbells-applied to early detection of myocardial infarction. Sensors Actuators B Chem 252:62–71

Negahdary M, Behjati-Ardakani M, Sattarahmady N, Heli H (2018) An aptamer-based biosensor for troponin I detection in diagnosis of myocardial infarction. J Biomed Phys Eng 8:167–178

Negahdary M, Behjati-Ardakani M, Heli H (2019a) An electrochemical troponin T aptasensor based on the use of a macroporous gold nanostructure. Microchim Acta 186:377

Negahdary M, Behjati-Ardakani M, Heli H, Sattarahmady N (2019b) A cardiac troponin T biosensor based on aptamer self-assembling on gold. Int J Mol Cell Med 8:271–283

Negahdary M, Sattarahmady N, Heli H (2020) Advances in prostate specific antigen biosensors-impact of nanotechnology. Clin Chim Acta 504:43–55

Nordström T, Akre O, Aly M, Grönberg H, Eklund M (2018) Prostate-specific antigen (PSA) density in the diagnostic algorithm of prostate cancer. Prostate Cancer Prostatic Dis 21:57–63

Öndeş B, Evli S, Uygun M, Aktaş Uygun D (2021a) Boron nitride nanosheet modified label-free electrochemical immunosensor for cancer antigen 125 detection. Biosens Bioelectron 191:113454

Öndeş B, Sinem E, Uygun M, Uygun DA (2021b) Boron nitride nanosheet modified label-free electrochemical immunosensor for cancer antigen 125 detection. Biosens Bioelectron 2021:113454

Pishvaian M, Morse MA, McDevitt J, Norton JD, Ren S, Robbie GJ, Ryan PC, Soukharev S, Bao H, Denlinger CS (2016) Phase 1 dose escalation study of MEDI-565, a bispecific T-cell engager that targets human carcinoembryonic antigen, in patients with advanced gastrointestinal adenocarcinomas. Clin Colorectal Cancer 15:345–351

Pumera M, Sanchez S, Ichinose I, Tang J (2007) Electrochemical nanobiosensors. Sensors Actuators B Chem 123:1195–1205

Putnin T, Waiwinya W, Pimalai D, Chawjiraphan W, Sathirapongsasuti N, Japrung D (2021) Dual sensitive and rapid detection of glycated human serum albumin using a versatile lead/graphene nanocomposite probe as a fluorescence–electrochemical aptasensor. Analyst 146:4357–4364

Qing M, Chen SL, Sun Z, Fan Y, Luo HQ, Li NB (2021) Universal and programmable rolling circle amplification-CRISPR/Cas12a-mediated immobilization-free electrochemical biosensor. Anal Chem 93:7499–7507

Rahi A, Sattarahmady N, Heli H (2016) Label-free electrochemical aptasensing of the human prostate-specific antigen using gold nanospears. Talanta 156–157:218–224

Raouafi A, Sánchez A, Raouafi N, Villalonga R (2019) Electrochemical aptamer-based bioplatform for ultrasensitive detection of prostate specific antigen. Sensors Actuators B Chem 297:126762

Rauf S, Lahcen AA, Aljedaibi A, Beduk T, Ilton de Oliveira Filho J, Salama KN (2021a) Gold nanostructured laser-scribed graphene: a new electrochemical biosensing platform for potential point-of-care testing of disease biomarkers. Biosens Bioelectron 180:113116

Rauf S, Mani V, Lahcen AA, Yuvaraja S, Beduk T, Salama KN (2021b) Binary transition metal oxide modified laser-scribed graphene electrochemical aptasensor for the accurate and sensitive screening of acute myocardial infarction. Electrochim Acta 386:138489

Reichlin T, Hochholzer W, Bassetti S, Steuer S, Stelzig C, Hartwiger S, Biedert S, Schaub N, Buerge C, Potocki M (2009) Early diagnosis of myocardial infarction with sensitive cardiac troponin assays. N Engl J Med 361:858–867

Ribeiro KL, Frías IAM, Silva AG, Lima-Neto RG, Sá SR, Franco OL, Oliveira MDL, Andrade CAS (2021) Impedimetric CLAVMO peptide-based sensor differentiates ploidy of *Candida* species. Biochem Eng J 167:107918

Romesser PB, Pei X, Shi W, Zhang Z, Kollmeier M, McBride SM, Zelefsky MJ (2018) Prostate-specific antigen (PSA) bounce after dose-escalated external beam radiation therapy is an independent predictor of PSA recurrence, metastasis, and survival in prostate adenocarcinoma patients. Int J Radiat Oncol Biol Phys 100:59–67

Rong S, Zou L, Li Y, Guan Y, Guan H, Zhang Z, Zhang Y, Gao H, Yu H, Zhao F, Pan H, Chang D (2021) An ultrasensitive disposable sandwich-configuration electrochemical immunosensor based on OMC@AuNPs composites and AuPt-MB for alpha-fetoprotein detection. Bioelectrochemistry 141:107846

Ropero-Vega JL, Redondo-Ortega JF, Galvis-Curubo YJ, Rondón-Villarreal P, Flórez-Castillo JM (2021) A bioinspired peptide in TIR protein as recognition molecule on electrochemical biosensors for the detection of *E. coli* O157:H7 in an aqueous matrix. Molecules 26:2559

Sajid KM, Parveen R, Sabih D, Chaouachi K, Naeem A, Mahmood R, Shamim R (2007) Carcinoembryonic antigen (CEA) levels in hookah smokers, cigarette smokers and non-smokers. J Pak Med Assoc 57:595

Sattarahmady N, Rahi A, Heli H (2017) A signal-on built in-marker electrochemical aptasensor for human prostate-specific antigen based on a hairbrush-like gold nanostructure. Sci Rep 7:1–8

Shafiei F, Saberi RS, Mehrgardi MA (2021) A label-free electrochemical aptasensor for breast cancer cell detection based on a reduced graphene oxide-chitosan-gold nanoparticle composite. Bioelectrochemistry 140:107807

Shamsazar A, Asadi A, Seifzadeh D, Mahdavi M (2021) A novel and highly sensitive sandwich-type immunosensor for prostate-specific antigen detection based on MWCNTs-Fe_3O_4 nanocomposite. Sensors Actuators B Chem 346:130459

Shanbhag MM, Ilager D, Mahapatra S, Shetti NP, Chandra P (2021) Amberlite XAD-4 based electrochemical sensor for diclofenac detection in urine and commercial tablets. Mater Chem Phys 273:125044

Shave R, Baggish A, George K, Wood M, Scharhag J, Whyte G, Gaze D, Thompson PD (2010) Exercise-induced cardiac troponin elevation: evidence, mechanisms, and implications. J Am Coll Cardiol 56:169–176

Shen M, Kan X (2021) Aptamer and molecularly imprinted polymer: synergistic recognition and sensing of dopamine. Electrochim Acta 367:137433

Siew QY, Pang EL, Loh H-S, Tan MTT (2021) Highly sensitive and specific graphene/TiO_2 impedimetric immunosensor based on plant-derived tetravalent envelope glycoprotein domain III (EDIII) probe antigen for dengue diagnosis. Biosens Bioelectron 176:112895

Smith DP, Calopedos R, Bang A, Yu XQ, Egger S, Chambers S, O'Connell DL (2018) Increased risk of suicide in New South Wales men with prostate cancer: analysis of linked population-wide data. PLoS One 13:e0198679

Song X, Zhao L, Luo C, Ren X, Yang L, Wei Q (2021) Peptide-based biosensor with a luminescent copper-based metal–organic framework as an electrochemiluminescence emitter for trypsin assay. Anal Chem 93:9704–9710

Spratt DE, Dai DL, Den RB, Troncoso P, Yousefi K, Ross AE, Schaeffer EM, Haddad Z, Davicioni E, Mehra R (2018) Performance of a prostate cancer genomic classifier in predicting metastasis in men with prostate-specific antigen persistence postprostatectomy. Eur Urol 74: 107–114

Sun Y, Fang L, Zhang Z, Yi Y, Liu S, Chen Q, Zhang J, Zhang C, He L, Zhang K (2021) A multitargeted electrochemiluminescent biosensor coupling DNAzyme with cascading amplification for analyzing myocardial miRNAs. Anal Chem 93:7516–7522

Taheri RA, Eskandari K, Negahdary M (2018) An electrochemical dopamine aptasensor using the modified Au electrode with spindle-shaped gold nanostructure. Microchem J 143:243–251

Tang H, Chen J, Nie L, Kuang Y, Yao S (2007) A label-free electrochemical immunoassay for carcinoembryonic antigen (CEA) based on gold nanoparticles (AuNPs) and nonconductive polymer film. Biosens Bioelectron 22:1061–1067

Tang H, Wang H, Yang C, Zhao D, Qian Y, Li Y (2020) Nanopore-based strategy for selective detection of single carcinoembryonic antigen (CEA) molecules. Anal Chem 92:3042–3049

Tao D, Wang J, Song S, Cai K, Jiang M, Cheng J, Hu L, Jaffrezic-Renault N, Guo Z, Pan H (2021a) Polythionine and gold nanostar-based impedimetric aptasensor for label-free detection of α-synuclein oligomers. J Appl Electrochem 51:1523–1533

Tao D, Wang J, Song S, Cai K, Jiang M, Cheng J, Hu L, Jaffrezic-Renault N, Guo Z, Pan H (2021b) Polythionine and gold nanostar-based impedimetric aptasensor for label-free detection of α-synuclein oligomers. J Appl Electrochem 51:e3

Tian J-K, Zhao M-L, Song Y-M, Zhong X, Yuan R, Zhuo Y (2021a) MicroRNA-triggered deconstruction of field-free spherical nucleic acid as an electrochemiluminescence biosensing switch. Anal Chem 93:13928–13934

Tian J, Liang Z, Hu O, He Q, Sun D, Chen Z (2021b) An electrochemical dual-aptamer biosensor based on metal-organic frameworks MIL-53 decorated with Au@Pt nanoparticles and enzymes for detection of COVID-19 nucleocapsid protein. Electrochim Acta 387:138553

Tran HL, Darmanto W, Doong R-A (2021) Electrochemical immunosensor for ultra-sensitive detection of attomolar prostate specific antigen with sulfur-doped graphene quantum dot@gold nanostar as the probe. Electrochim Acta 389:138700

Villalonga A, Estabiel I, Pérez-Calabuig AM, Mayol B, Parrado C, Villalonga R (2021) Amperometric aptasensor with sandwich-type architecture for troponin I based on carboxyethylsilanetriol-modified graphene oxide coated electrodes. Biosens Bioelectron 183:113203

Wang C, Li J, Kang M, Huang X, Liu Y, Zhou N, Zhang Z (2021a) Nanodiamonds and hydrogen-substituted graphdiyne heteronanostructure for the sensitive impedimetric aptasensing of myocardial infarction and cardiac troponin I. Anal Chim Acta 1141:110–119

Wang J-M, Yao L-Y, Huang W, Yang Y, Liang W-B, Yuan R, Xiao D-R (2021b) Overcoming aggregation-induced quenching by metal−organic framework for electrochemiluminescence (ECL) enhancement: Zn-PTC as a new ECL emitter for ultrasensitive microRNAs detection. ACS Appl Mater Interfaces 13:44079–44085

Wang W, Han R, Tang K, Zhao S, Ding C, Luo X (2021c) Biocompatible peptide hydrogels with excellent antibacterial and catalytic properties for electrochemical sensing application. Anal Chim Acta 1154:338295

Wang X-Y, Feng Y-G, Wang A-J, Mei L-P, Luo X, Xue Y, Feng J-J (2021d) Facile construction of ratiometric electrochemical immunosensor using hierarchical PtCoIr nanowires and porous SiO_2@Ag nanoparticles for accurate detection of septicemia biomarker. Bioelectrochemistry 140:107802

Wu G, Datar RH, Hansen KM, Thundat T, Cote RJ, Majumdar A (2001) Bioassay of prostate-specific antigen (PSA) using microcantilevers. Nat Biotechnol 19:856–860

Xiang B, Snook AE, Magee MS, Waldman SA (2013) Colorectal cancer immunotherapy. Discov Med 15:301

Xiao K, Meng L, Du C, Zhang Q, Yu Q, Zhang X, Chen J (2021) A label-free photoelectrochemical biosensor with near-zero-background noise for protein kinase A activity assay based on porous ZrO_2/CdS octahedra. Sensors Actuators B Chem 328:129096

Xie X, Wang Z, Zhou M, Xing Y, Chen Y, Huang J, Cai K, Zhang J (2021) Redox host–guest nanosensors installed with DNA gatekeepers for immobilization-free and ratiometric electrochemical detection of miRNA. Small Methods 5:2101072

Yang L, Wang J, Lü H, Hui N (2021) Electrochemical sensor based on Prussian blue/multi-walled carbon nanotubes functionalized polypyrrole nanowire arrays for hydrogen peroxide and microRNA detection. Microchim Acta 188:25

Yazdani Z, Yadegari H, Heli H (2019) A molecularly imprinted electrochemical nanobiosensor for prostate specific antigen determination. Anal Biochem 566:116–125

Zhang F, Liu Z, Han Y, Fan L, Guo Y (2021a) Sandwich electrochemical carcinoembryonic antigen aptasensor based on signal amplification of polydopamine functionalized graphene conjugate Pd-Pt nanodendrites. Bioelectrochemistry 142:107947

Zhang J, Zhang X, Gao Y, Yan J, Song W (2021b) Integrating CuO/g-C_3N_4 p-n heterojunctioned photocathode with MoS_2 QDs@Cu NWs multifunctional signal amplifier for ultrasensitive detection of AβO. Biosens Bioelectron 176:112945

Zhang Q, Li W, Zhao F, Xu C, Fan G, Liu Q, Zhang X, Zhang X (2021c) Electrochemical sandwich-type thrombin aptasensor based on silver nanowires & particles decorated electrode and the signal amplifier of Pt loaded hollow zinc ferrite. Colloids Surf A Physicochem Eng Asp 611:125804

Zhao S, Liu N, Wang W, Xu Z, Wu Y, Luo X (2021) An electrochemical biosensor for alpha-fetoprotein detection in human serum based on peptides containing isomer D-amino acids with enhanced stability and antifouling property. Biosens Bioelectron 190:113466

Zheng J, Zhao H, Ning G, Sun W, Wang L, Liang H, Xu H, He C, Zhao H, Li C-P (2021) A novel affinity peptide–antibody sandwich electrochemical biosensor for PSA based on the signal amplification of MnO_2-functionalized covalent organic framework. Talanta 233:122520